Journal of Catalysis 269 (2010) 291–301

Contents lists available at ScienceDirect

Journal of Catalysis

journal homepage: www.elsevier.com/locate/jcat

Competitive adsorption of nitrogen species in HDS: Kinetic characterization of hydrogenation and hydrogenolysis sites

Teh C. Ho *, Liang Qiao [1]

Corporate Strategic Research Labs., ExxonMobil Research and Engineering Co., Annandale, NJ 08801, United States

ARTICLE INFO

Article history:
Received 28 August 2009
Revised 6 November 2009
Accepted 11 November 2009
Available online 24 December 2009

Keywords:
Hydrodesulfurization
Hydrodenitrogenation
Hydrogenation
Hydrogenolysis
Competitive adsorption
Active site density
Dibenzothiophenes
Carbazoles

ABSTRACT

Through modeling of the transient response of dibenzothiophene (DBT) hydrodesulfurization (HDS) to inhibition by 3-ethylcarbazole (3ECBZ), the hydrogenation (HYA) and hydrogenolysis (HYL) functions of a sulfided $CoMo/Al_2O_3–SiO_2$ catalyst are characterized. The HYL sites, accounting for about one third of the total active sites, have a lower adsorption affinity for 3ECBZ than for DBT. The opposite is true for the HYA sites. The adsorbed nitrogen species are denitrogenated more rapidly on the HYL sites than on the HYA sites. As a result, the HYL sites are less inhibited by 3ECBZ and drive the HDS of DBT almost single-handedly in the presence of 3ECBZ. The catalyst surface is sparsely occupied by sulfur species because the HDS rate is much faster than the hydrodenitrogenation rate on both HYA and HYL sites. These results give a quantitative understanding of why 3ECBZ is a far weaker inhibitor to the HDS of DBT than it is to the HDS of 4,6-diethyldibenzothiophene. There appears a tradeoff between the HYA and HYL functions, which can be exploited for HDS catalyst and process optimization.

1. Introduction

Driven by the growing demand for ultraclean fuels and the increasing use of heavy oils, sulfur removal from fossil oils has received and will continue to attract much attention in the coming years. Tremendous efforts have been expended on the discovery and development of new catalytic or noncatalytic (e.g., adsorption, oxidation) technologies for sulfur reduction, as evidenced by the voluminous patent and scientific literature. Currently, the most effective technology remains the hydrodesulfurization (HDS) process using $Co(Ni)MoS_2(WS_2)$ catalysts [1–3]. These catalysts desulfurize dibenzothiophene (DBT) and its alkyl derivatives via two pathways. As Fig. 1 shows, the hydrogenolysis (HYL) path produces biphenyl (BP), whereas the hydrogenation (HYA) path gives cyclohexylbenzene (CHB) [4]. The latter involves ring hydrogenation followed by hydrogenolytic cleavage of the C–S bond [5]. The former has also been referred to as the direct desulfurization (DDS) path. We do not adopt this nomenclature because the present work is about simultaneous HDS and hydrodenitrogenation (HDN). The term DDS does not have a clear meaning for the HDN of nitrogen heterocycles such as carbazoles.

The nanostructure of HDS catalysts is notoriously difficult to characterize. The active sites are generally believed to be sulfur vacancies associated with Mo (or W) cations and SH^-/S^{2-} groups on the edges and corners of MoS_2 (WS_2) crystallites [1,2]. Some of the Mo cations are substituted by the promoter metals Co or Ni. Many possible structural configurations with varying degree of coordinative unsaturation can exist, each having its own activity/selectivity for HYA and HYL. Recently, nonvacancy sites have also been identified. They are metallic brim sites with remarkable hydrogenation function [6,7]. A detailed mathematical modeling of this state of affairs at the reactor scale is all but impossible. It is necessary to retreat to an averaging approach that lumps various active sites into just one or two types. A dual-site model can differentiate HYA and HYL functions based on product distribution.

Competitive adsorption among organosulfur (S), organonitrogen (N), and aromatic compounds is a critical issue in hydroprocessing catalyst/process research and development. In the HDS of middle distillates (200–370 °C boiling range; diesel, jet fuel, heating oil, etc.), the sulfur removal rate becomes increasingly inhibited by N species as the extent of desulfurization gets increasingly deeper [8–10]. Organonitrogen species are the most potent inhibitor when it comes to desulfurizing hindered alkyldibenzothiophenes comprising 4-substituted and 4,6-disubstituted dibenzothiophenes [8]. In addition to blocking the active sites for HDS, the adsorbed N compounds would slow down the hydrogen activation process, thus limiting the supply of surface hydrogen for

* Corresponding author.
E-mail address: teh.c.ho@exxonmobil.com (T.C. Ho).
[1] Present address: Mount Sinai School of Medicine, Annenberg 20-84B, Box 1137, East 100th Street and Madison Ave., New York, NY 10029, United States.

0021-9517/$ - see front matter © 2009 Elsevier Inc. All rights reserved.
doi:10.1016/j.jcat.2009.11.012

Nomenclature

B	concentration of biphenyl in the fluid phase
C	concentration of cyclohexylbenzene in the fluid phase
b	defined as B/S_f
c	defined as C/S_f
g	$k_n N_f/k_{HDN}$
g_ℓ	defined in Eq. (46)
g_τ	defined in Eq. (46)
h_a	$k_{sa}S_f/k_{HDSa}$
h_ℓ	$k_{s\ell}S_f/k_{HDS\ell}$
k_{HDS}	surface HDS rate constant (s^{-1})
k_{HDN}	surface HDN rate constant (s^{-1})
k_n	adsorption rate constant for nitrogen (cc liquid feed/s/μmol)
k_s	adsorption rate constant for sulfur (cc liquid feed/s/μmol)
k'_n	desorption rate constant for nitrogen (s^{-1})
k'_s	desorption rate constant for sulfur (s^{-1})
L	reactor length (3.82 cm)
m_a	defined in Eq. (A7)
m_ℓ	defined in Eq. (A8)
N	concentration of nitrogen atom in the fluid phase (μmol/cc feed)
n	N/N_f
N_f	feed nitrogen atom concentration (5.76×10^{-5} g N atom/cc or 4.1 μmol/cc)
q_m	catalyst active site density (μmol/g cat)
q_s	concentration of adsorbed sulfur atom on catalyst (μmol/g cat)
q_n	concentration of adsorbed nitrogen atom on catalyst (μmol/g cat)
S	concentration of sulfur atom in the fluid phase (μmol/cc liquid feed)
S_f	feed sulfur atom concentration (1.88×10^{-3} g S/cc or 58.8 μmol/cc feed)
s	S/S_f
$\hat{s}$	s at Steady State I
$\bar{s}$	s at Steady State II
t	time
v	superficial velocity based on empty tube
w_a	defined in Eq. (A5)
w_ℓ	defined in Eq. (A6)
z	axial distance from the entrance of the reactor (cm)

Greek letters

α_ℓ	defined in Eq. (A1)
α_a	defined in Eq. (A2)
β_a	defined in Eq. (A3)
β_ℓ	defined in Eq. (A4)
ε	bed void fraction (0.3)
θ	q/q_m, fractional coverage of adsorbed species
ρ_p	catalyst particle density (1.15 g cat/cc cat)
ζ	$t/(L\varepsilon/v)$
ξ	z/L

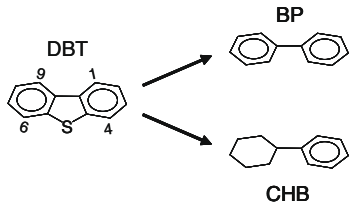

Fig. 1. A simplified DBT HDS reaction scheme; BP, biphenyl; CHB, cyclobenzene.

hydroprocessing reactions [11,12]. Moreover, N-heterocycles are known to have a high tendency to form coke, thereby shortening catalyst lifetime [12,13].

Many difficult-to-desulfurize refinery feedstocks have a significant amount of five-membered nitrogen heterocycles such as alkylcarbazoles, which are hard to denitrogenate [9,12,14]. While N-inhibition effects have been a well-studied subject, most prior kinetic studies were conducted under steady-state conditions. The data were usually analyzed with a single-site Langmuir-Hinshelwood model in which surface reactions are assumed to be rate limiting and the adsorption and desorption are quasi-equilibrated. Very few dual-site models have been reported in the literature (e.g., [15–18]).

To develop means of mitigating N-inhibition requires a quantitative understanding of the inhibition dynamics. A most effective way to achieve this goal is by a combined experimental and modeling study of the transient response of the catalyst to a well-defined stimulus generated by reaction probes in a flow reactor. In doing so, one can quantify the active site density and the associated rate constants. This approach was used to characterize a commercial sulfided $CoMo/Al_2O_3$–SiO_2 catalyst with a probe consisting of 4,6-diethyldibenzothiophene (46DEDBT) and 3-ethylcarbazole (3ECBZ). In terms of active site requirements, these two probe molecules align with each other in that their hydroremoval reactions rely primarily on the HYA function [10,19]. Thus, as a first approximation, a single-site model was used to analyze the inhibition dynamics by treating all sites as if they were of the HYA type [20,21].

A major motivation for this study was the following observation. The HDS rate of 46DEDBT over $CoMo/Al_2O_3$–SiO_2 decreases precipitously upon addition of a trace amount of 3ECBZ (5 wppm as N atom) to the feed; yet the HDS of DBT is only moderately inhibited by 80 wppm feed N [19]. To understand these remarkably different inhibiting behaviors, here we examine the inhibition dynamics using a probe consisting of DBT and 3ECBZ. These two molecules have very different requirements for active sites: the HDS of DBT predominately follows the HYL route, while the HDN of 3ECBZ relies heavily on the HYA pathway. Accordingly, the present work develops a dual-site model capable of distinguishing HYA and HYL sites. The model gives a quantitative picture of the dynamic interactions between DBT and 3ECBZ and explains why DBT HDS is more N resistant than 46DEDBT HDS. It also reveals an HYA–HYL tradeoff whose practical implications are discussed with examples taken from experiments with petroleum fractions.

2. Experimental

The details of the experimental procedures are available elsewhere [19]. What follows is a brief description of some key aspects. The $CoMo/Al_2O_3$–SiO_2 catalyst (3 g), in the form of 20/40-mesh granules, was presulfided at 400 °C for one hour at atmospheric pressure with a 10% H_2S-in-H_2 mixture. A cocurrent fixed-bed reactor, made of a nominal 3/8-inch ID 316 stainless steel pipe, was operated isothermally in up-flow mode to avoid incomplete catalyst wetting and bypassing. The reaction conditions were 265 °C, 3 WHSV (liquid weight hourly space velocity), 1.83 MPa hydrogen pressure, and 116 cc H_2/cc liquid feed. Axial dispersion

was minimized through dilution with 3 g of glass beads. The variation of the hydrogen pressure across the reactor is insignificant.

The transient experiments entail tracking changes in catalyst behavior following a step jump in the feed nitrogen concentration. Specifically, the experiments were started with a feed containing 1.5 wt% DBT to obtain the baseline data in the absence of 3ECBZ. After the catalyst lined out its activity (Steady State I), the feed was switched over to one that contains 1.5 wt% DBT and 0.112 wt% 3ECBZ (80 wppm total nitrogen) at the same reaction conditions. The state of the reactor is monitored by intermittently analyzing the liquid products at the reactor outlet until the catalyst reached Steady State II. Modeling the thus-obtained data offers an effective means of discriminating among rival models and estimating catalyst site densities as well as associated rate constants.

The density of the liquid feed is 0.72 g/cc. The liquid products were identified and quantified by GC/MS and GC using a 75% OV1/25% SW-10-fused silica capillary column. Acetone was used as the internal standard. Besides H_2S, the dominant HDS products by far were cyclohexylbenzenes (CHB) and biphenyls (BP). Trace amounts of tetrahydrodibenzothiophene (THDBT), bicyclohexyl (BCH), and benzylcyclopentane were noted. The total nitrogen content in the liquid effluent was measured by combustion and chemiluminescence using the Antek analyzer. Due to their low concentrations, individual HDN products were not measured. The carrier solvent dodecane is essentially inert under the reaction conditions studied.

3. Experimental results

3.1. HDS reaction pathways

As Fig. 2 shows, the product mass ratio γ_{DBT} = [CHB]/[BP] (the square bracket denotes the wt% in the liquid product) is a weak increasing function of the extent of HDS (or 1/WHSV). This indicates a rather slow hydrogenation of BP to CHB [22,23]. The hydrogenation of CHB to bicyclohexyl is even slower because CHB is much less reactive than BP [22]. Thus, for practical purposes, the HDS of DBT can be approximated as two independent reactions as shown in Fig. 1 in which transitory intermediates and kinetically insignificant pathways are neglected.

Fig. 2 also indicates that at high DBT conversions (>80% HDS), $\gamma_{DBT} \approx 0.3$. By contrast, the HDS of 46DEDBT over the same catalyst gives γ_{DEDBT} = [C4CHB]/[C4BP] > 5, with [C4BP] and [C4CHB] being the concentrations of diethylbiphenyls and diethylcyclohexylbenzenes, respectively [19]. The big difference between the two γ values reinforces the notion that there is little overlap in terms of active site requirements for the HDS of DBT and 46DEDBT in the absence of N inhibitors. Put differently, the DBT-HDS and 46DEDBT-HDS systems are nearly "orthogonal" to each other. Indeed, there is very little mutual inhibition in simultaneous HDS of DBT and 46DMDBT [24].

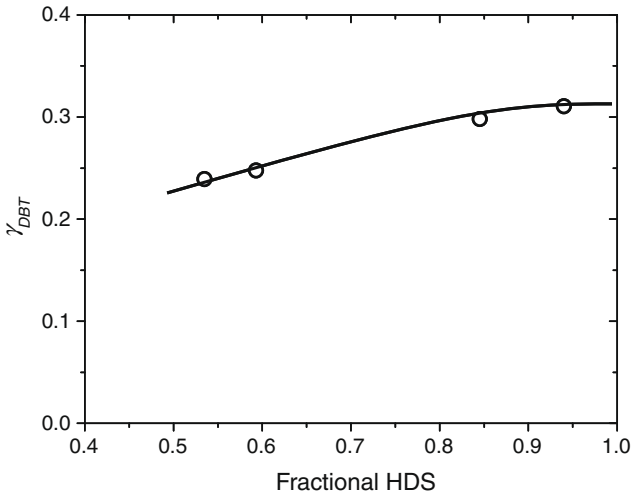

Fig. 2. γ_{DBT} vs. fractional HDS; 1.83 MPa, 265 °C, 116 cc H_2/cc liquid feed, and varying WHSV; sulfided CoMo/Al_2O_3–SiO_2.

3.2. Transient response

Fig. 3 displays the results of the inhibition experiment. The HDS level declines from 95% at Steady State I to 64% at Steady State II after the N adsorption front completely passes through the bed. The inhibition transient has a characteristic time scale of about 50 h, which is much longer than the fluid residence time inside the reactor. The time scale for N desorption is even longer [19].

As shown in Fig. 3, a large fraction of the active sites in the HDS of DBT are spared from the 3ECBZ assault. For perspective, the figure also shows that at the same level of feed nitrogen (80 wppm), 3ECBZ has a catastrophic effect on the HDS of 46DEDBT – with HDS plummeting from 70% to less than 10%. As reported previously [19], the 46DEDBT HDS level drops from 70% to 34% with a feed nitrogen concentration as low as 5 wppm. This was rationalized by positing that the HDS of 46DEDBT requires specific multiplets of adjacent sulfur vacancies that are surrounded by readily available SH^- groups. These sites, having special geometric and/or electronic properties, become totally incapacitated upon chemisorption of even a trace amount of 3ECBZ. This "structure-sensitive" inhibition is not observed in the HDS of DBT. Real feed experiments have also shown that indigenous N species are far more effective in inhibiting hindered DBTs than in inhibiting unhindered DBTs [25,26].

Fig. 4 shows that γ_{DBT} declines sharply during the N breakthrough period. While both HYA and HYL sites are inhibited, there is a disproportionately greater decrease in the CHB concentration than in the BP concentration. So the HYL sites have a higher capacity to resist the jump in N concentration. In other words, the inhibition is selective in that the HYA function is suffered more than the HYL function.

4. Model development

We now construct a mathematical model for estimating the site density and rate constants from the data obtained during the

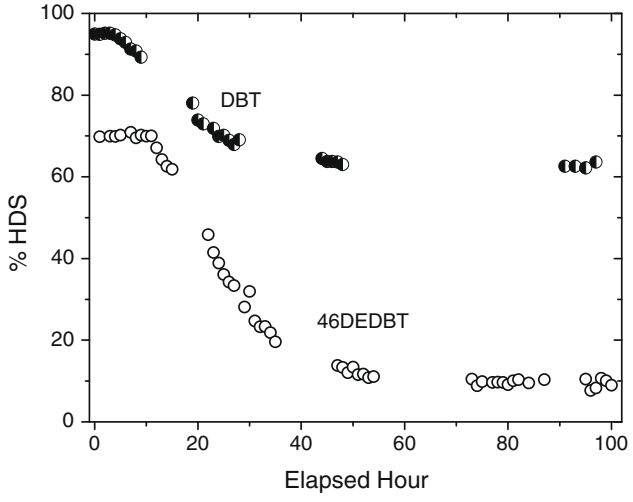

Fig. 3. Percentages of HDS of DBT and 46DEDBT at reactor exit as functions of elapsed time following introduction of 3-ethylcarbazole; 265 °C, 1.83 MPa, 116 cc H_2/cc liquid feed, 2.4 WHSV (for 46DEDBT HDS), 3.0 WHSV (for DBT HDS).

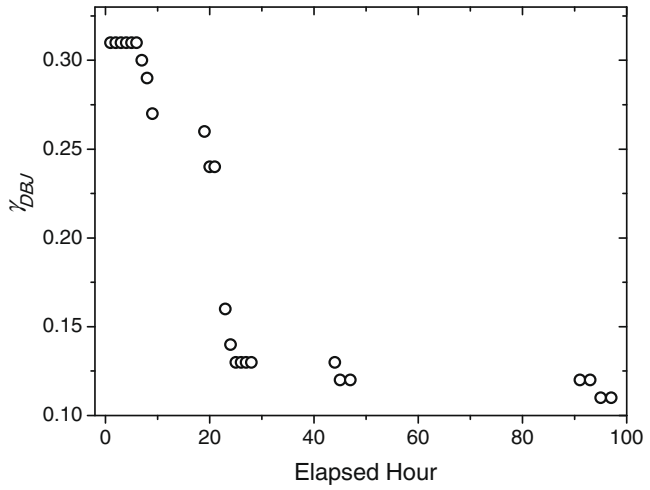

Fig. 4. γ_{DBT} vs. elapsed time; 1.83 MPa, 265 °C, 116 cc H_2/cc liquid feed, 3 WHSV.

breakthrough period and at Steady States I and II. All active sites are lumped into either the HYA or HYL type. All nitrogen-containing species (3ECBZ and its HDN intermediates) and sulfur-containing species (DBT and its HDS intermediates) are grouped as N-compounds and S-compounds, respectively. Let S and N be the sulfur atom and nitrogen atom concentrations in the flowing stream, respectively. The concentrations of BP and CHB are represented by B and C, respectively. The subscripts a and l signify quantities associated with the HYA and HYL sites, respectively. We denote q_{na} as the adsorbed nitrogen (atom) concentration on the HYA sites, $q_{s\ell}$ as the adsorbed sulfur concentration on the HYL sites, and q_{ma} as the saturated chemisorption capacity of the HYA sites. Then $\theta_{na} \equiv q_{na}/q_{ma}$ is the fractional coverage of the adsorbed nitrogen on the HYA sites. The same applies to $q_{m\ell}$ and $\theta_{n\ell} \equiv q_{nl}/q_{m\ell}$. Here we use the sulfur and nitrogen species to "sample" (or "titrate") the active sites (adsorbed BP and CHB are much smaller than adsorbed S and N). So q_{ma} and $q_{m\ell}$ are a measure of catalyst's HYA and HYL maximum site densities, respectively.

For HDS, k_s, k_s', and k_{HDS} are the adsorption rate constant, desorption rate constant, and surface HDS rate constant, respectively. Likewise, the corresponding rate constants for HDN are k_n, k_n', and k_{HDN}. And the rate constants for BP and CHB are k_b, k_b', k_c, and k_c', respectively. The sulfur and nitrogen atom concentrations in the feed are denoted by S_f and N_f, respectively. Reactor specifications are: bed void fraction, $\varepsilon = 0.3$; catalyst particle density, $\rho_p = 1.15$ g/cc; bed length, $L = 3.82$ cm; and superficial fluid velocity based on empty reactor, $v = 2.63 \times 10^{-3}$ cm/s. The average fluid velocity in the interstices between particles is v/ε.

4.1. Full model

Before setting out the model equations, we make the following simplifying assumptions. (1) The catalyst surface is Langmuirian and energetically uniform; (2) hydrogen is adsorbed on sites that are different from those for S and N adsorption; (3) due to the high hydrogen/DBT volume ratio, the hydrogen pressure is constant and the surface hydrogen coverage is high; (4) the effect of molar change due to reaction is negligible; (5) the inhibiting effects of H_2S, NH_3, and heteroatom-free hydrocarbons are relatively insignificant compared to that of 3ECBZ; (6) axial dispersion effect and the velocity changes due to adsorption are negligible; (7) the concentrations of S- and N-compounds are constant throughout the catalyst particles; (8) the reactor is isothermal and isobaric, with negligible mass transfer effects; (9) HDS and HDN both occur irreversibly on the catalyst surface and hydrogen addition is not rate limiting; (10) catalyst deactivation by coking is negligible over the time scale of the experiment; and (11) liquid feed and hydrogen reach physical equilibrium before entering the catalyst bed. With these assumptions, we write the following mass balance equations for a plug-flow reactor.

(1) Mass balance of S in the fluid phase and on HYA and HYL sites

$$\varepsilon\frac{\partial S}{\partial t} + v\frac{\partial S}{\partial z} = -(1-\varepsilon)\rho_p[k_{sa}S(q_{ma}-q_{sa}-q_{na}) + k_{s\ell}S(q_{m\ell}-q_{s\ell}-q_{n\ell}) - k'_{sa}q_{sa} - k'_{s\ell}q_{s\ell}] \quad (1)$$

$$\frac{\partial q_{sa}}{\partial t} = k_{sa}S(q_{ma}-q_{sa}-q_{na}) - k'_{sa}q_{sa} - k_{HDSa}q_{sa} \quad (2)$$

$$\frac{\partial q_{s\ell}}{\partial t} = k_{s\ell}S(q_{m\ell}-q_{s\ell}-q_{n\ell}) - k'_{s\ell}q_{s\ell} - k_{HDS\ell}q_{s\ell} \quad (3)$$

(2) Mass balance of N in the fluid phase and on HYA and HYL sites

$$\varepsilon\frac{\partial N}{\partial t} + v\frac{\partial N}{\partial z} = -(1-\varepsilon)\rho_p[k_{na}N(q_{ma}-q_{sa}-q_{na}) + k_{n\ell}N(q_{m\ell}-q_{s\ell}-q_{n\ell}) - k'_{na}q_{na} - k'_{n\ell}q_{n\ell}] \quad (4)$$

$$\frac{\partial q_{na}}{\partial t} = k_{na}N(q_{ma}-q_{sa}-q_{na}) - k'_{na}q_{na} - k_{HDNa}q_{na} \quad (5)$$

$$\frac{\partial q_{n\ell}}{\partial t} = k_{n\ell}N(q_{m\ell}-q_{s\ell}-q_{n\ell}) - k'_{n\ell}q_{n\ell} - k_{HDN\ell}q_{n\ell} \quad (6)$$

(3) Mass balance of BP in the fluid phase and on HYA and HYL sites

$$\varepsilon\frac{\partial B}{\partial t} + v\frac{\partial B}{\partial z} = -(1-\varepsilon)\rho_p[k_{ba}B(q_{ma}-q_{sa}-q_{na}) + k_{b\ell}B(q_{m\ell}-q_{s\ell}-q_{n\ell}) - k'_{ba}q_{ba} - k'_{b\ell}q_{b\ell}] \quad (7)$$

$$\frac{\partial q_{ba}}{\partial t} = k_{ba}B(q_{ma}-q_{sa}-q_{na}) - k'_{ba}q_{ba} \quad (8)$$

$$\frac{\partial q_{b\ell}}{\partial t} = k_{b\ell}B(q_{m\ell}-q_{s\ell}-q_{n\ell}) - k'_{b\ell}q_{b\ell} + k_{HDS\ell}q_{s\ell} \quad (9)$$

(4) Mass balance of CHB in the fluid phase and on HYA and HYL sites

$$\varepsilon\frac{\partial C}{\partial t} + v\frac{\partial C}{\partial z} = -(1-\varepsilon)\rho_p[k_{ca}C(q_{ma}-q_{sa}-q_{na}) + k_{c\ell}C(q_{m\ell}-q_{s\ell}-q_{n\ell}) - k'_{ca}q_{ca} - k'_{c\ell}q_{c\ell}] \quad (10)$$

$$\frac{\partial q_{ca}}{\partial t} = k_{ca}C(q_{ma}-q_{sa}-q_{na}) - k'_{ca}q_{ca} + k_{HDSa}q_{sa} \quad (11)$$

$$\frac{\partial q_{c\ell}}{\partial t} = k_{c\ell}C(q_{m\ell}-q_{s\ell}-q_{n\ell}) - k'_{c\ell}q_{c\ell} \quad (12)$$

Note that the differentiation of HYA and HYL sites is based on the concentrations of BP and CHB in the liquid product.

4.2. Model reduction

To construct a simplest possible model necessitates further pruning so the dimensionality of the parameter space is reduced. This is achieved via time scale separation [20,27]. For example, the slow desorption of N-compounds can be considered as frozen over the time scale of the inhibition transient. At the other extreme, the surface HDS is too fast to influence the sluggish inhibition process ($k_{HDS} \gg k_{HDN}$ because the C–S bond is much weaker than the C–N bond). The consequence is that the inhibition transient is mainly governed by the interplay of sulfur adsorption, nitrogen adsorption, and surface HDN. It is relevant to mention that experiments using industrial feedstocks have also shown that the desorptions of N-compounds [28] and S-compounds [29] are slow.

In light of the above, we set $k'_{na} \ll k_{na}N_f$, $k'_{n\ell} \ll k_{n\ell}N_f$, $k'_{na} \ll k_{HDNa}$, $k'_{n\ell} \ll k_{HDN\ell}$, $k'_{sa} \ll k_{HDSa}$, and $k'_{s\ell} \ll k_{HDS\ell}$.

A further stipulation is that the surface HDS rate is faster than the adsorption rate so that $k_{sa}S_f \ll k_{HDSa}$ and $k_{s\ell}S_f \ll k_{HDS\ell}$. The

desorptions of N- and S-compounds are not fast enough to attain a local adsorption–desorption equilibrium as the N- and S-adsorption fronts travel down the bed during the breakthrough period.

It is also reasonable to stipulate that $q_{s\ell} \ll q_{n\ell}$ and $q_{sa} \ll q_{na}$ based on the following order-of-magnitude arguments. At steady state and with the assumption of slow desorption, it follows from Eqs. (2), (3), (5), and (6) that

$$\frac{q_{sa}}{q_{na}} = \left(\frac{k_{sa}}{k_{na}}\right)\left(\frac{k_{HDNa}}{k_{HDSa}}\right)\left(\frac{S}{N}\right), \qquad \frac{q_{s\ell}}{q_{n\ell}} = \left(\frac{k_{s\ell}}{k_{n\ell}}\right)\left(\frac{k_{HDN\ell}}{k_{HDS\ell}}\right)\left(\frac{S}{N}\right) \tag{13}$$

Let $S/N \sim S_f/N_f = O(10^2)$. From the 46DEDBT–3ECBZ probe [20,21], we estimate that $(k_{sa}/k_{na})_{46DEDBT-3ECBZ} = O(10^{-1})$ and $(k_{HDNa}/k_{HDSa})_{46DEDBT-3ECBZ} = O(10^{-6})$, implying that $(q_{sa}/q_{na})_{46DEDBT-3ECBZ} \sim O(10^{-5})$. Due to DBT's higher k_{HDS}, we expect that $(k_{HDN}/k_{HDS})_{DBT-3ECBZ} < (k_{HDN}/k_{HDS})_{46DEDBT-3ECBZ}$ on both HYA and HYL sites. Also, the ratio $(k_{s\ell}/k_{n\ell})_{DBT-3ECBZ}$ should be higher than or comparable to $(k_{sa}/k_{na})_{DBT-3ECBZ}$. And the ratio $(k_{sa}/k_{na})_{DBT-3ECBZ}$ is expected not to be greater than $(k_{sa}/k_{na})_{46DEDBT-3ECBZ}$ by more than, say, two orders of magnitude (to be confirmed *a posteriori*). These arguments lead to the supposition that $(q_{sa}/q_{na})_{DBT-3ECBZ} \ll 1$ and $(q_{s\ell}/q_{n\ell})_{DBT-3ECBZ} \ll 1$. Finally, we suppose that over the time window of the inhibition transient, the surface concentrations of BP and CHB are both at a quasi-steady state ($\partial q_{ba}/\partial t \approx 0$, $\partial q_{b\ell}/\partial t \approx 0, \partial q_{ca}/\partial t \approx 0$, and $\partial q_{c\ell}/\partial t \approx 0$). We are left with a much simplified model (six equations instead of 12)

$$\varepsilon\frac{\partial S}{\partial t} + v\frac{\partial S}{\partial z} = -(1-\varepsilon)\rho_p[k_{sa}S(q_{ma}-q_{na}) + k_{s\ell}S(q_{m\ell}-q_{n\ell})] \tag{14}$$

$$\varepsilon\frac{\partial N}{\partial t} + v\frac{\partial N}{\partial z} = -(1-\varepsilon)\rho_p[k_{na}N(q_{ma}-q_{na}) + k_{n\ell}N(q_{m\ell}-q_{n\ell})] \tag{15}$$

$$\frac{\partial q_{na}}{\partial t} = k_{na}N(q_{ma}-q_{na}) - k_{HDNa}q_{na} \tag{16}$$

$$\frac{\partial q_{n\ell}}{\partial t} = k_{n\ell}N(q_{m\ell}-q_{n\ell}) - k_{HDN\ell}q_{n\ell} \tag{17}$$

$$\varepsilon\frac{\partial B}{\partial t} + v\frac{\partial B}{\partial z} = (1-\varepsilon)\rho_p k_{s\ell}S(q_{m\ell}-q_{n\ell}) \tag{18}$$

$$\varepsilon\frac{\partial C}{\partial t} + v\frac{\partial C}{\partial z} = (1-\varepsilon)\rho_p k_{sa}S(q_{ma}-q_{na}) \tag{19}$$

Here the active sites are primarily occupied by adsorbed N species, which are the driver of the inhibition dynamics.

To identify governing parameters, Eqs. (14)–(19) are made dimensionless with the following scaled variables: $s = S/S_f$, $n = N/N_f$, $b = B/S_f$, $c = C/S_f$, $\xi = z/L$, and $\varsigma = t/(L\varepsilon/v)$. Note that WHSV = $v/[(1-\varepsilon)\rho_p L]$. The inhibition process comprises many competing events. A mathematical description of the system should reflect the relative time scales of these events, which are defined by the following dimensionless groups (see the Appendix for details): $\alpha_\ell = k_{s\ell}q_{m\ell}/WHSV$, $\alpha_a = k_{sa}q_{ma}/WHSV$, $\beta_a = k_{na}q_{ma}/WHSV$, $\beta_\ell = k_{n\ell}q_{m\ell}/WHSV$, $w_a = k_{na}N_f/(L\varepsilon/v)$, $w_\ell = k_{n\ell}N_f/(L\varepsilon/v)$, $m_a = k_{HDNa}(L\varepsilon/v)$, $m_\ell = k_{HDN\ell}(L\varepsilon/v)$, $g_a = w_a/m_a = k_{na}N_f/k_{HDNa}$, and $g_\ell = w_\ell/m_\ell = k_{n\ell}N_f/k_{HDN\ell}$.

With the above dimensionless quantities, Eqs. (14)–(19) in dimensionless form become

$$\frac{\partial s}{\partial \varsigma} + \frac{\partial s}{\partial \xi} = -[\alpha_\ell s(1-\theta_{n\ell}) + \alpha_a s(1-\theta_{na})] \tag{20}$$

$$\frac{\partial n}{\partial \varsigma} + \frac{\partial n}{\partial \xi} = -[\beta_a n(1-\theta_{na}) + \beta_\ell n(1-\theta_{n\ell})] \tag{21}$$

$$\frac{\partial \theta_{na}}{\partial \varsigma} = w_a n(1-\theta_{na}) - m_a\theta_{na} \tag{22}$$

$$\frac{\partial \theta_{n\ell}}{\partial \varsigma} = w_\ell n(1-\theta_{n\ell}) - m_\ell\theta_{n\ell} \tag{23}$$

$$\frac{\partial b}{\partial \varsigma} + \frac{\partial b}{\partial \xi} = \alpha_\ell s(1-\theta_{n\ell}) \tag{24}$$

$$\frac{\partial c}{\partial \varsigma} + \frac{\partial c}{\partial \xi} = \alpha_a s(1-\theta_{na}) \tag{25}$$

To solve the above equations we need to specify the boundary conditions at $\xi = 0$ and the initial conditions at $\zeta = 0$. At $\xi = 0$, $s = n = 1$ and $b = c = 0$ for $\zeta > 0$. Moreover, at $\xi = 0$

$$\frac{d\tilde{\theta}_{na}}{d\varsigma} = w_a n(1-\tilde{\theta}_{na}) - m_a\tilde{\theta}_{na} \tag{26}$$

$$\frac{d\tilde{\theta}_{n\ell}}{d\varsigma} = w_\ell n(1-\tilde{\theta}_{n\ell}) - m_\ell\tilde{\theta}_{n\ell} \tag{27}$$

where $\tilde{\theta}_{na}(\varsigma) = \theta_{na}(0,\varsigma)$ and $\tilde{\theta}_{n\ell}(\varsigma) = \theta_{n\ell}(0,\varsigma)$. Eqs. (26) and (27) require the initial conditions $\tilde{\theta}_{na} = \tilde{\theta}_{n\ell} = 0$ at $\zeta = 0$.

There are eight independent dimensionless groups in the governing equations. We next specify the initial conditions for Eqs. (20)–(25) and derive five constraints from analysis of the steady states. The present dual-site model thus has three adjustable parameters. By contrast, the previous single-site model has only one fitting parameter [20].

4.3. Steady State I (DBT feed)

The initial condition $\zeta = 0$ ($\xi \geqslant 0$) for the model corresponds to the steady state of the reactor prior to the inhibition experiment. At this steady state, we let $s = \hat{s}$, $b = \hat{b}$, and $c = \hat{c}$. Also, $n = \theta_{na} = \theta_{n\ell} = 0$ and

$$\frac{d\hat{s}}{d\xi} = -(\alpha_\ell + \alpha_a)\hat{s} \tag{28}$$

$$\frac{d\hat{b}}{d\xi} = \alpha_\ell\hat{s}, \quad \frac{d\hat{c}}{d\xi} = \alpha_a\hat{s} \tag{29}$$

At $\xi = 0$, $\hat{s} = 1$ and $\hat{b} = \hat{c} = 0$. The above equations can then be integrated to give

$$\hat{s} = e^{-(\alpha_\ell+\alpha_a)\xi} \tag{30}$$

$$\hat{b} = \frac{\alpha_\ell}{\alpha_\ell+\alpha_a}[1-e^{-(\alpha_\ell+\alpha_a)\xi}] \tag{31}$$

$$\hat{c} = \frac{\alpha_a}{\alpha_\ell+\alpha_a}[1-e^{-(\alpha_\ell+\alpha_a)\xi}] \tag{32}$$

Note that $\hat{s} + \hat{b} + \hat{c} = 1$. The constraints imposed by Steady State I are the measured concentrations of DBT, BP, and CHB at the reactor exit. It can be seen from Eq. (30) that the exponential decay of DBT is dictated by adsorption (α_ℓ and α_a). Let $\hat{b} = b_1$ and $\hat{c} = c_1$ at $\xi = 1$, both of which are obtained experimentally. The result is that α_ℓ and α_a can be determined from the data obtained at Steady State I

$$\alpha_\ell = \frac{b_1}{b_1+c_1}\ln\frac{1}{1-(b_1+c_1)} \tag{33}$$

$$\alpha_a = \frac{c_1}{b_1+c_1}\ln\frac{1}{1-(b_1+c_1)} \tag{34}$$

4.4. Steady State II (DBT + 3ECBZ feed)

After a sufficiently long time, the system under N inhibition relaxes to Steady State II. That is, in the limit of $\zeta \to \infty$, Eqs. (20)–(25) revert to the governing equations for Steady State II at which $s = \bar{s}$, $n = \bar{n}$, $b = \bar{b}$, $c = \bar{c}$, and $\theta = \bar{\theta}$. The governing equations are

$$\frac{d\bar{s}}{d\xi} = -[\alpha_a(1-\bar{\theta}_{na}) + \alpha_\ell(1-\bar{\theta}_{n\ell})]\bar{s} \tag{35}$$

$$\frac{d\bar{n}}{d\xi} = -[\beta_a(1-\bar{\theta}_{na}) + \beta_\ell(1-\bar{\theta}_{n\ell})]\bar{n} \tag{36}$$

$$0 = w_a\bar{n}(1-\bar{\theta}_{na}) - m_a\bar{\theta}_{na} \tag{37}$$

$$0 = w_\ell\bar{n}(1-\bar{\theta}_{n\ell}) - m_\ell\bar{\theta}_{n\ell} \tag{38}$$

$$\frac{d\bar{b}}{d\xi} = \alpha_\ell(1-\bar{\theta}_{n\ell})\bar{s} \tag{39}$$

$$\frac{d\bar{c}}{d\xi} = \alpha_a(1-\bar{\theta}_{na})\bar{s} \tag{40}$$

It follows from Eqs. (37) and (38) that

$$\bar{\theta}_{na} = \frac{g_a \bar{n}}{1 + g_a \bar{n}}, \quad \bar{\theta}_{n\ell} = \frac{g_\ell \bar{n}}{1 + g_\ell \bar{n}} \tag{41}$$

Steady State II is then defined by the following dual-site model

$$\frac{d\bar{s}}{d\bar{\xi}} = -\left(\frac{\alpha_\ell}{1 + g_\ell \bar{n}} + \frac{\alpha_a}{1 + g_a \bar{n}}\right)\bar{s} \tag{42}$$

$$\frac{d\bar{n}}{d\bar{\xi}} = -\left(\frac{\beta_\ell}{1 + g_\ell \bar{n}} + \frac{\beta_a}{1 + g_a \bar{n}}\right)\bar{n} \tag{43}$$

$$\frac{d\bar{b}}{d\bar{\xi}} = \frac{\alpha_\ell(1 - \bar{b} - \bar{c})}{1 + g_\ell \bar{n}} \tag{44}$$

$$\frac{d\bar{c}}{d\bar{\xi}} = \frac{\alpha_a(1 - \bar{b} - \bar{c})}{1 + g_a \bar{n}} \tag{45}$$

The foregoing equations were solved numerically with boundary conditions at $\bar{\xi} = 0$: $\bar{s}(0) = \bar{n}(0) = 1$ and $\bar{b}(0) = \bar{c}(0) = 0$. The exit concentrations measured at $\bar{\xi} = 1$ provide three additional constraints: $\bar{n}(1) = n_2$, $\bar{b}(1) = b_2$, and $c(1) = c_2$ are required to match the experimental data. Thus, the total number of adjustable parameters is reduced from eight to three. The two dimensionless parameters α_ℓ and α_a in Eqs. (28) and (42) can be viewed as effective HDS rate constants for the HYL and HYA sites in the presence of 3ECBZ, respectively. Similarly, from Eqs. (42)–(45), we note that the severity of 3ECBZ inhibition can be gauged by the two dimensionless parameters g_a and g_ℓ [20]

$$g_a = \frac{k_{na} N_f}{k_{HDNa}}, \qquad g_\ell = \frac{k_{n\ell} N_f}{k_{HDN\ell}} \tag{46}$$

The g's are nothing but the ratio of the nitrogen adsorption rate to the surface HDN rate. The surface coverage of N-compounds depends on the surface HDN rate (k_{HDN}). Alkylcarbazoles are strong inhibitors because of their fast adsorption coupled with slow HDN [12,14,20].

4.5. Parameter estimation

The parameter estimation was carried out through a two-stage optimization with constraints derived from steady-state experiments. As parameters α_ℓ and α_a can be determined through Steady State I (Section 4.3), formally, six adjustable parameters (Eqs. (A3)–(A8) in the Appendix) are subject to optimization. However, there are three implicit, nonlinear algebraic constraints imposed by Steady State II. Therefore, in essence, only three of the six parameters are free. The objective function to be minimized is the Euclidean norm of the difference (in the form a vector) between experimental data obtained at the reactor exit and the corresponding model predictions as functions of time. It is reasonable to use the single-site model parameters as initial guesses for the corresponding parameters in the dual-site model. This is so because the behavior of the N-compounds in the presence of DBT should not be vastly different from that in the presence of 46DEDBT [20,21]. With the one-site model parameters as the base point, we construct a six-dimensional parameter space around the base point, in which each of the six parameters can vary over a 25-fold range. We then use a global optimization algorithm to minimize the objective function within this six-dimensional parameter space subject to three nonlinear constraints. The thus-found optimal parameter set was used as an initial guess for a local optimization algorithm to find the final optimal parameter set. All the computations were performed in MATLAB. The global and local optimizations were conducted using the subroutines "glcSolve" and "fmincon" in the commercial package TOMLAB, respectively.

Table 1
DBT HDS dual-site model: rate constants and site densities.

Parameter	Units	Value
k_{na}	cc liquid feed/s/μmol	1.5×10^{-5}
$k_{n\ell}$	cc liquid feed/s/μmol	8.7×10^{-6}
k_{HDNa}	s^{-1}	7.3×10^{-6}
$k_{HDN\ell}$	s^{-1}	1.6×10^{-5}
k_{sa}	cc liquid feed/s/μmol	8.6×10^{-6}
$k_{s\ell}$	cc liquid feed/s/μmol	5.3×10^{-5}
q_{ma}	μmol N adatom/g cat	157.1
$q_{m\ell}$	μmol N adatom/g cat	85.7

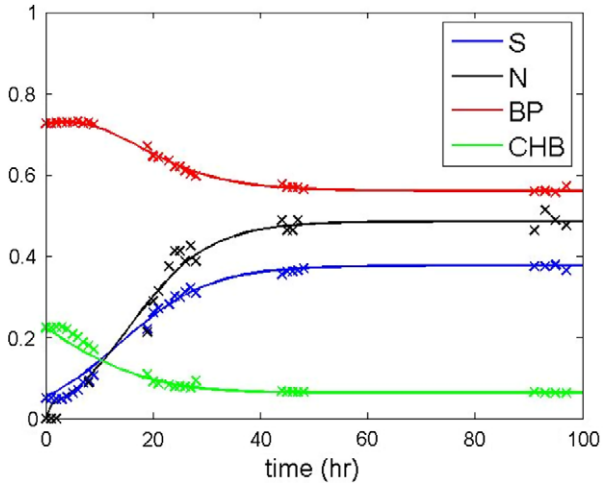

Fig. 5. Dimensionless concentrations s, n, b, and c at reactor exit as functions of elapsed time; 265 °C, 3 WHSV, 1.83 MPa, and 116 cc H_2/cc liquid feed. Solid lines are model predictions. Symbols are experimental results.

5. Results and discussions

5.1. Comparison with experiment

The rate parameters and saturated chemisorption capacities estimated from the present dual-site model are listed in Table 1. Since the catalytic sites are almost completely occupied by N species, the site densities q_{ma} and $q_{m\ell}$ can be identified with the concentration of chemisorbed nitrogen, with the units being μmol N adatom/g cat. The model parameters in Table 1 are used to compute the solid curves shown in Fig. 5. As can be seen, the predicted behaviors compare well with measured exit (relative or dimensionless) concentrations of different species (s, n, b, and c) as functions of elapsed hour after introducing the 3ECBZ-containing feed. The model captures the dominant features of the inhibition dynamics.

5.2. Spatiotemporal behavior

Fig. 6 depicts the normalized sulfur concentration in the fluid phase as a function of bed position and elapsed time. Initially, in the absence of 3ECBZ, the sulfur profile shows an exponential decline. Then the sulfur concentration in the reactor effluent increases as the inhibition proceeds. Compared with the HDS of 46DEDBT, here 3ECBZ is a benign inhibitor; a significant level of sulfur removal can still be achieved at Steady State II.

Fig. 7 shows the corresponding behavior of the nitrogen concentration in the fluid phase. The speed at which the organonitrogen wave travels through the bed is far slower than the superficial velocity of the fluid. Here the shape of the wave front is dictated by the combined action of adsorption and surface HDN. For

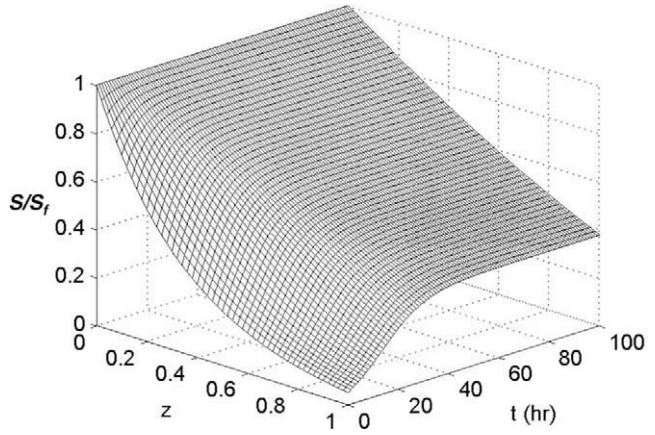

Fig. 6. Spatiotemporal behavior of S/S_f; 1.83 MPa, 265 °C, 116 cc H_2/cc liquid feed, and 3 WHSV.

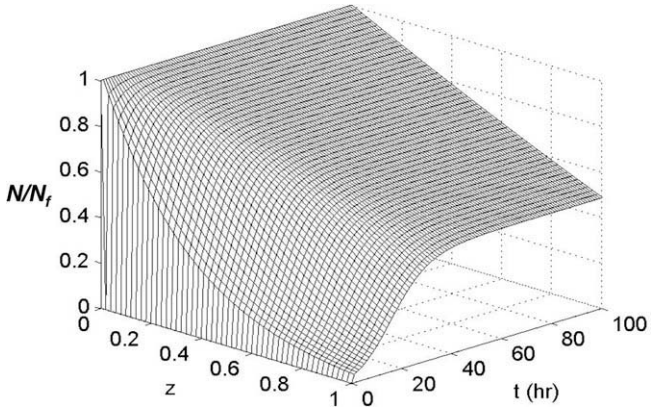

Fig. 7. Spatiotemporal behavior of N/N_f; 1.83 MPa, 265 °C, 116 cc H_2/cc liquid feed, and 3 WHSV.

illustration, we only show the spatiotemporal behavior of θ_{na} in Fig. 8. At the reactor inlet, θ_{na} increases sharply and then levels off. Here θ_{na} is order of unity; despite this, the extent of DBT HDS is still respectably high because an enough fraction of HYL sites remain active.

Although the model ignores both θ_{sa} and $\theta_{s\ell}$, one can estimate them by assuming $\partial q_{sa}/\partial t \approx \partial q_{s\ell}/\partial t \approx 0$, $k'_{sa} \ll k_{HDSa}$, and $k'_{s\ell} \ll k_{HDS\ell}$. It then follows that

$$\theta_{sa} = \frac{h_a s(1-\theta_{na})}{1+h_a s}, \quad \theta_{s\ell} = \frac{h_\ell s(1-\theta_{n\ell})}{1+h_\ell s} \tag{47}$$

where $h_a = k_{sa}S_f/k_{HDSa}$ and $h_\ell = k_{s\ell}S_f/k_{HDS\ell}$. Fig. 9 depicts the behavior of θ_{sa} whose maximum occurs at the reactor entrance. When N species arrive, delodging of S species starts to occur near the reactor entrance. The sulfur species in the fluid phase then have to go further downstream to search for bare HYA sites. As a result, the maximum moves from the reactor inlet toward the bed interior and eventually reaches the reactor outlet. An observer standing at the reactor outlet will notice that θ_{sa} goes through a maximum as time goes by. The behavior of $\theta_{s\ell}$ is similar. Both θ_{sa} and $\theta_{s\ell}$ are small, the presence of DBT has little impact on the extent of the HDN of 3ECBZ. As expected, the behavior shown in Fig. 9 is qualitatively similar to that predicted for the 46DEDBT–3ECBZ probe [21].

5.3. HYL vs. HYA sites

This section aims to contrast the HYA and HYL sites based on the transient responses of the $CoMo/Al_2O_3$–SiO_2 catalyst to two

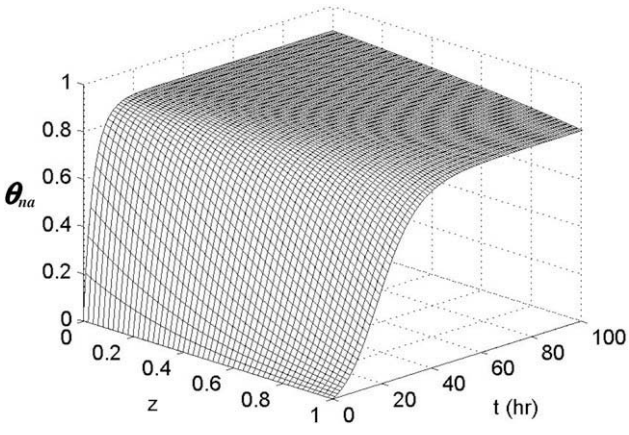

Fig. 8. Spatiotemporal behavior of θ_{na}; 1.83 MPa, 265 °C, 116 cc H_2/cc liquid feed, and 3 WHSV.

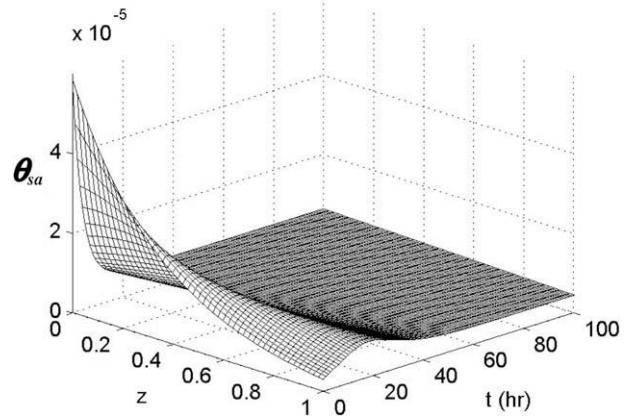

Fig. 9. Spatiotemporal behavior of θ_{sa}; 1.83 MPa, 265 °C, 116 cc H_2/cc liquid feed, and 3 WHSV.

"orthogonal" probes: DBT and 46DEDBT with 3ECBZ as the common inhibitor. The DBT–3ECBZ probe provides information on both HYL and HYA sites. The previous single-site model for the 46DEDBT–3ECBZ probe rests on the assumption that all sites perform the HYA function [20]. On this point, it bears emphasizing that we lump various active sites into HYA and HYL types; each type is a collection of different sites that presumably share some common features. For example, one proposition has been that the HYA pathway prefers the π adsorption, whereas the HYL pathway involves the σ adsorption [5]. Tables 1 and 2 list the active site densities and overall rate constants estimated from the two probes.

5.3.1. Adsorption of N species

Referring to Table 1, one notices that $k_{s\ell} \gg k_{sa}$, which is in keeping with the notion that DBT desulfurization relies heavily on the HYL function. Although the adsorption of DBT on HYA sites is relatively slow, it is comparable to that of 46DEDBT (see Table 2). The adsorption of N species, on the other hand, exhibits the opposite behavior: $k_{n\ell} < k_{na}$. We take the results of density functional theory calculations [30] as suggesting that the adsorption of 3ECBZ on HYA sites favors the flat configuration (η^6-coordination) through the π-electrons of a condensed carbocyclic ring. As for the chemisorption of 3ECBZ on HYL sites, we venture to propose that the initial mode of contact may involve a Lewis basic site and the NH group of the pyrrolic ring [31]. This proposition is based on the notion that the N–H bond in 3ECBZ is liable and

Table 2
46DEDBT HDS single-site model: rate constants and site density.

Parameter	Units	Value
k_{na}	cc liquid feed/s/μmol	2.7×10^{-5}
k_{HDNa}	s^{-1}	6.3×10^{-6}
k_{sa}	cc liquid feed/s/μmol	6.7×10^{-6}
q_{ma}	μmol N adatom/g cat	271.4

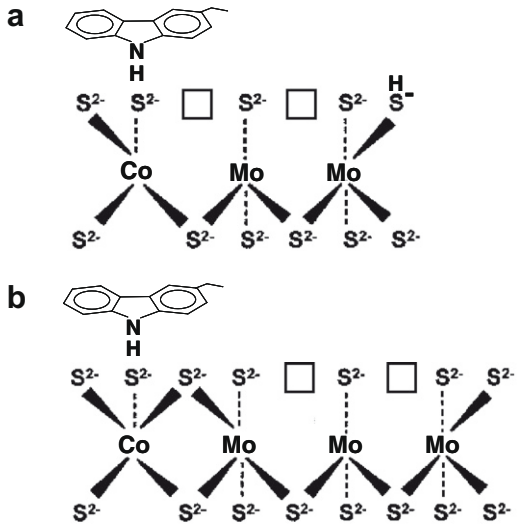

Fig. 10. Possible adsorption mode for 3-ethylcarbazole on the edge of Co-promoted MoS_2; (□), sulfur vacancy.

deprotonation may possibly take place on a basic S^{-2} site. The presence of Co and Ni would strengthen the basicity (or "mobility", loosely speaking) of S^{-2} species [32] and hence facilitate the deprotonation process. Fig. 10 illustrates two possible scenarios. This argument is in line with the facts that the metal-S bonds are weaker in CoMo and NiMo sulfides than in Mo sulfide [33] and that Co/Ni would increase sulfur's electron density [34]. The upshot here is that while the flat, η^6-coordination may be the preferred chemisorption mode, there may exist an alternative, secondary chemisorption mode involving deprotonation of the NH group.

5.3.2. Adsorption selectivity and surface HDN rate

The difference in adsorption characteristics between HYL and HYA sites can be further quantified by contrasting their adsorption affinities for S species relative to those for N species. The DBT–3ECBZ probe gives the adsorption selectivities for HYL and HYA sites

$$p_\ell = \frac{k_{s\ell}}{k_{n\ell}} = 6.1 > 1 \qquad p_a = \frac{k_{sa}}{k_{na}} = 0.57 < 1 \tag{48}$$

Thus, the HYL sites are about ten times more selective toward DBT adsorption than are the HYA sites. When it comes to adsorption on the HYL sites, 3ECBZ cannot compete with DBT. On the other hand, the HYA sites adsorb 3ECBZ faster than they adsorb DBT. From Tables 1 and 2, one can see that the p values obtained from the two probes justify the assumption $q_{s\ell} \ll q_{n\ell}$ and $q_{sa} \ll q_{na}$.

Since the desorption of N-compounds is negligibly slow over the time scale of interest, the surface coverage by N-compounds is dictated by k_{HDN}, which plays the role of cleaning up the surface. The dual-site model reveals that $k_{HDN\ell} > k_{HDNa}$. It thus appears that while the adsorption of 3ECBZ on the HYL sites is relatively slow ($k_{n\ell} < k_{na}$), the denitrogenation rate is facile once 3ECBZ becomes adsorbed via the aforementioned deprotonation step. The resulting anionic pyrrole-like nitrogen could interact with an exposed Mo ion electronically, leading to a facile C–N bond cleavage.

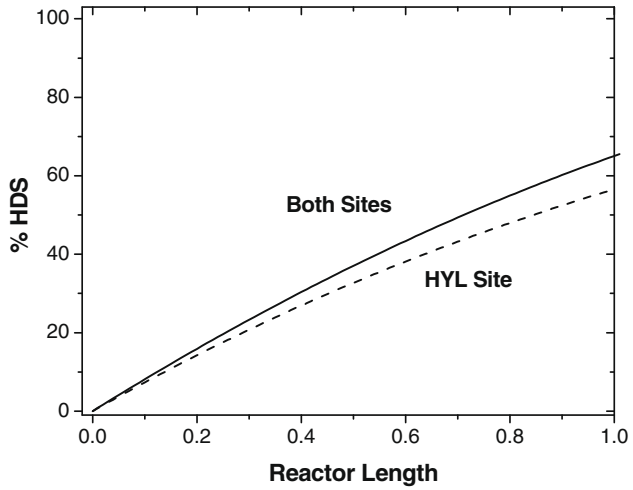

Fig. 11. Percent HDS as a function of fractional reactor bed length in the presence of 3-ethylcarbazole, Steady State II.

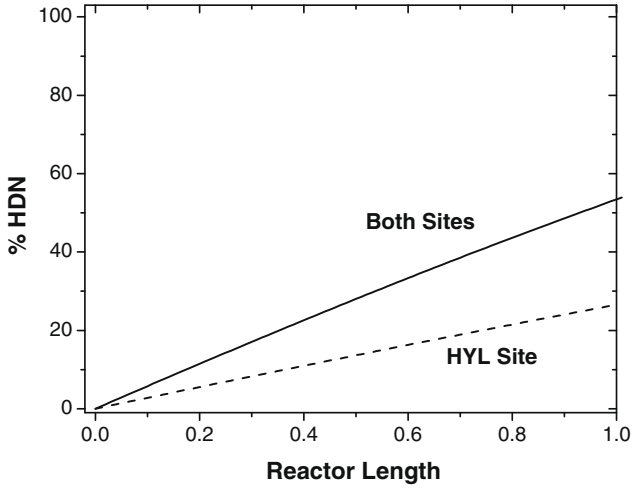

Fig. 12. Percent HDN as a function of fractional reactor bed length in the presence of 3-ethylcarbazole, Steady State II.

5.3.3. Inhibition severity

The overall effect of the interplay of adsorption and surface reaction can be quantified by the inhibition severity g defined by Eq. (46). From the DBT–3ECBZ probe, we have

$$\frac{g_a}{g_\ell} = 3.8 \tag{49}$$

Hence, the inhibition severity on the HYA sites is about four times that on the HYL sites. This is consistent with the steep decline of γ_{DBT} shown in Fig. 4. Since $\theta_n \propto k_n/k_{HDN}$, we have $\theta_{n\ell} < \theta_{na}$. The low k_n/k_{HDN} ratio of the HYL sites dampens the impact of 3ECBZ inhibition. This, coupled with the fact that $\alpha_\ell > \alpha_a$, indicates that in the presence of 3ECBZ, the HYL sites essentially desulfurize DBT single-handedly. This is shown in Fig. 11, which is obtained from integrating Eq. (42) using the parameters listed in Table 1. Fig. 12, obtained from integrating Eq. (43), shows that the HYL sites are as important as the HYA sites even in the HDN of 3ECBZ.

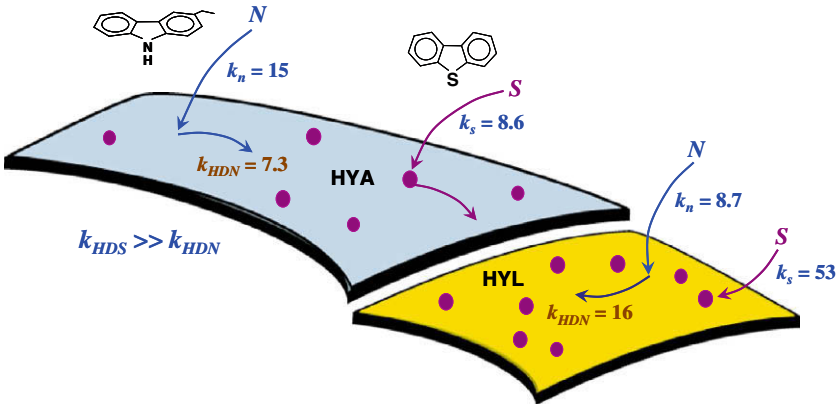

Fig. 13. Schematic showing that the inhibition dynamics is governed by S adsorption, N adsorption, and surface HDN reactions on HYA and HYL sites. Rate constants are on a relative scale.

For perspective, the single-site model for 46DEDBT desulfurization indicates that the inhibition is more severe, with $g_{a,46DEDBT}/g_{a,DBT} = 2.1$. This was referred to as a case of "structure-sensitive" inhibition in Section 3.2. Note also that HDN is self-inhibited, as indicated by Eq. (43). The k_{na} and k_{HDNa} listed in Table 2 should be viewed as apparent values reflecting the underlying assumption that all sites are of the HYA type.

The forgoing discussions, taken together, rationalize why the inhibition impact on the HDS of DBT is far less than that on the HDS of 46DEDBT. The DBT HDS relies primarily on the HYL sites whose low k_n/k_{HDN} ratio makes it less vulnerable to 3ECBZ attack than the HYA sites.

5.3.4. Active site density

We now turn to the density of active sites. As Table 1 shows, the DBT–3ECBZ probe coupled with the dual-site model "sees" a total site density of about 243 μmol N adatom/g cat, about one third of which is associated with the HYL function. By comparison, the 46DEDBT–3ECBZ probe coupled with the one-site model gives a comparable total site density of 272 μmol N adatom/g cat. It must be pointed out that comparing site density and distribution should introduce a certain degree of dependence on the probe molecule. This arises from the fact that the structure and electronic states of active sites can be strongly influenced by the probe molecule. And the reaction environments (e.g., local H_2/H_2S ratio, etc.) generated from two distinctly different probe molecules can be very different due to dynamic surface reconstruction, which may lead to interconversion between the two types of sites. Our premise here is that the DBT and 46DEDBT probes molecules give high "resolutions" for the HYL and HYA functions, respectively.

5.3.5. Summary of inhibition dynamics

Kinetically complex catalyst systems often have many widely disparate time scales. Fortunately, seldom does the need for considering all of them arise. This characteristic allows model developers to focus only on events that are kinetically significant within the time scale of interest. The present dual-site model is developed in this spirit. Fig. 13 is a schematic showing that the inhibition dynamics is governed by S adsorption, N adsorption, and surface HDN reactions on HYA and HYL sites. The relative sizes of the two site types reflect their relative densities. The key differences between the HYL and HYA sites in the HDS of DBT are $k_{s\ell} \gg k_{sa}$, $k_{n\ell} < k_{na}$, and $k_{HDN\ell} > k_{HDNa}$. There is one thing in common: both types of sites are almost completely occupied by N species ($\theta_{s\ell} \ll \theta_{n\ell}$, $\theta_{sa} \ll \theta_{na}$) because $k_{HDS} \gg k_{HDN}$. While the adsorption of 3ECBZ is nonselective, its inhibiting impacts on the HYA and HYL sites are very different. The surface coverage of S species is very low (represented by solid purple dots), with the HYL sites having a higher coverage than the HYA sites.

6. Hydrogenation–hydrogenolysis tradeoff

We may infer from the foregoing discussions that there appears a tradeoff between HYA and HYL functions in the following sense. Although the HYA sites are desirable because of their intrinsically high activity for desulfurizing hindered DBTs, they are very vulnerable to N-inhibition. On the other hand, the HYL sites, notwithstanding their low activity for the HDS of hindered DBTs, have the advantage of being more resistant to N-inhibition. The following two examples address the question of whether the tradeoff can be exploited to advantage.

6.1. Catalyst splitting strategy

The example here has to do with deep HDS of light catalytic cycle oil (LCO), which is a most difficult-to-desulfurize middle distillate. The idea is to develop a catalyst-zoning strategy that plays the strength of two catalysts with very different selectivities. One catalyst is a bulk (unsupported) $Ni_{0.5}Mn_{0.5}Mo$ sulfide that has a very high selectivity toward HYA (high γ). In fact, the catalyst is so HYA-selective that it desulfurizes 4DEDBT faster than it desulfurizes DBT [9]. The other catalyst is commercial sulfided $CoMo/Al_2O_3$, which is far more HYL-selective than $Ni_{0.5}Mn_{0.5}Mo$ sulfide. The HDS activity of the bulk catalyst is more sensitive to N-inhibition than that of the supported CoMo catalyst. As detailed elsewhere [9,35], a most profitable way of using these two catalysts is to place $Ni_{0.5}Mn_{0.5}Mo$ sulfide downstream of $CoMo/Al_2O_3$ in a stacked-bed reactor. The overall HDS and HDN performances of a 50/50 stacked bed are far superior to those obtained from the weighted sum of the activities of the constituent catalysts, thus signifying a synergism. Apparently, even a modest HDN level attained by $CoMo/Al_2O_3$ can significantly dampen the N inhibition impacts on the downstream bulk catalyst. The high HYA function of the bulk catalyst makes it relatively insensitive to the H_2S generated from the $CoMo/Al_2O_3$ catalyst [9]. It should be pointed out that the stacked-bed outperforms a 50/50 bed in which the two catalysts were mixed uniformly, even though the latter also exhibits an activity synergism [36].

The reverse 50/50 stacked-bed ($Ni_{0.5}Mn_{0.5}Mo$ is upstream of $CoMo/Al_2O_3$) also gives rise to a synergism, albeit a weaker one [35]. In this case, the HYA sites on the bulk catalyst play a sacrificial role in protecting the downstream $CoMo/Al_2O_3$ catalyst from N inhibition. This stacking order is suboptimal because the

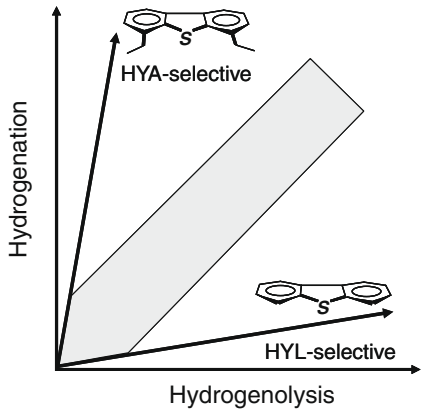

Fig. 14. For deep HDS, the required catalyst properties are high hydrogenation activity combined with high resistance to N inhibition. The latter requires hydrogenolysis functionality. Conceptually, the desired catalysts lie inside the gray area that represents the optimum compromise between two opposing requirements.

$CoMo/Al_2O_3$ catalyst has a lower sensitivity to N inhibition and hence does not need much protection.

The above results suggest that the perceived refractoriness of 4-substituted and 4,6-disubstituted DBTs may well stem from the high vulnerability of the HYA sites to N-inhibition, rather than from a lack of reactivity. Fig. 14 shows that the DBT-HDS and 46DEDBT-HDS systems are nearly orthogonal to each other because the former requires a highly HYL-selective catalyst, while the latter requires a highly HYA-selective catalyst. For deep HDS, the required catalyst properties are a sufficiently high HYA activity combined with a sufficiently high resistance to N inhibition. An optimum catalyst system then represents the best possible compromise between the two opposing requirements. Conceptually, such an optimum system may lie intermediate between the two limits, which is schematically represented by the gray area shown in Fig. 14. The foregoing stacked-bed approach is in line with this reasoning. As an aside, bulk metal sulfide catalysts generally have a higher HYA selectivity (higher γ) than Al_2O_3-supported metal sulfide catalysts [9,10].

6.2. Feed splitting strategy

While the above example is about catalyst splitting, the example here is about feedstock splitting. An LCO was fractionated into two boiling cuts: 340 °C-minus and 340 °C-plus [37]. The 340 °C-minus cut mainly comprises benzothiophenes, DBT, one- to three-ring aromatics, and indoles/quinolines. The 340 °C-plus cut largely comprises alkyl-DBTs, four$^+$-ring aromatics, and carbazoles. These two boiling cuts were desulfurized over a sulfided $CoMo/Al_2O_3$ and a sulfided $NiMo/Al_2O_3$ catalysts. The former should be more HYL-selective than the latter.

It turned out that $CoMo/Al_2O_3$ outperformed $NiMo/Al_2O_3$ in the deep HDS of the more refractory 340 °C-plus cut. The reverse is true for the deep HDS of the 340 °C-minus cut. This may be interpreted as arising from the fact that the HYL-selective $CoMo/Al_2O_3$ catalyst is less vulnerable to inhibition by carbazoles. The implication then is that it may be preferable to use $CoMo/Al_2O_3$, instead of $NiMo/Al_2O_3$, for deep HDS of middle distillates under conditions that are difficult for the HYA sites to excel (e.g., low hydrogen pressures).

7. Conclusions

In a previous study, a single-site model was developed to understand the dynamics of adsorption competition between 46DEDBT and 3ECBZ on a sulfided $CoMo/Al_2O_3$–SiO_2 catalyst. The present work develops a non-equilibrium, dual-site model that quantitatively delineates the competition between DBT and 3ECBZ over the same catalyst under transient and steady-state conditions. According to this probe reaction, one third of the active sites are associated with the HYL function, with the balance being the HYA sites. It is suggested that Co(Ni)-enhanced basic sites comprising S^{-2} species could be involved in the initial adsorption of alkylcarbazoles via deprotonation of the NH group. The HYA sites have a stronger adsorption affinity for 3ECBZ than for DBT. The opposite is true for the HYL sites. This, coupled with the faster HDN turnover rate on the HYL sites, dampens the 3ECBZ inhibition effect on the HYL sites. These results explain why DBT HDS is much less susceptible to N inhibition than 46DEDBT HDS and point to the importance of the HYL sites in the deep HDS of middle distillates. To mitigate the N-inhibiting effect, an active deep HDS catalyst requires a delicate balance between HYA and HYL functions.

The present modeling study invokes several simplifying assumptions. To obtain more detailed information, some of the assumptions need to be relaxed. One such example is the neglect of irreversible poisoning of the active sites. On this point, we remark that in the HDS of DBT, the inhibition by 1,10-phenanthroline is reversible on the HYL sites, but not on the HYA sites [38].

The present study suggests that standardized model-compound experiments under transient conditions are quite useful for kinetic characterization of HDS catalysts and rational interpretation/reconciliation of results obtained from model-compound and real-feed experiments. The two probes, DBT/3ECBZ and 46DEDBT/3ECBZ, are suitable for this purpose for covering the deep HDS regime. Further work should also include polynuclear aromatics as probe molecules. The approach developed here provides a framework that allows a more quantitative characterization of multifunctional HDS catalysts than has been reported hitherto.

Acknowledgment

This work was carried out while Liang Qiao was a summer student visitor from the Department of Chemical Engineering at Princeton University.

Appendix A. System dimensionless groups

As mentioned in the text, the system dimensionless groups reflect the relative time scales of various events underlying the inhibition process.

$$\alpha_\ell = \frac{1/WHSV}{(1/k_{s\ell}q_{m\ell})} = \frac{\text{space time based on catalyst weight}}{\text{time scale for full } S \text{ adsorption on HYL sites}} \tag{A1}$$

$$\alpha_a = \frac{1/WHSV}{(1/k_{sa}q_{ma})} = \frac{\text{space time based on catalyst weight}}{\text{time scale for full } S \text{ adsorption on HYA sites}} \tag{A2}$$

$$\beta_a = \frac{1/WHSV}{(1/k_{na}q_{ma})} = \frac{\text{space time based on catalyst weight}}{\text{time scale for full } N \text{ adsorption on HYA sites}} \tag{A3}$$

$$\beta_\ell = \frac{1/WHSV}{(1/k_{n\ell}q_{m\ell})} = \frac{\text{space time based on catalyst weight}}{\text{time scale for full } N \text{ adsorption on HYL sites}} \tag{A4}$$

$$w_a = \frac{L\varepsilon/v}{1/(k_{na}N_f)} = \frac{\text{fluid residence time}}{\text{time scale for } N \text{ local adsorption on HYA sites}} \tag{A5}$$

$$w_\ell = \frac{L\varepsilon/v}{1/(k_{n\ell}N_f)} = \frac{\text{fluid residence time}}{\text{time scale for } N \text{ local adsorption on HYL sites}} \tag{A6}$$

$$m_a = \frac{L\varepsilon/v}{1/k_{HDNa}} = \frac{\text{fluid residence time}}{\text{time scale for HDN reaction on HYA sites}} \tag{A7}$$

$$m_\ell = \frac{L\varepsilon/v}{1/k_{HDN\ell}} = \frac{\text{fluid residence time}}{\text{time scale for HDN reaction on HYL sites}} \tag{A8}$$

Note that w_a, w_ℓ, m_a, and m_ℓ are various forms of the Damköhler number. There are four derived dimensionless groups: $p_a = \alpha_a/\beta_a = k_{sa}/k_{na}$, $p_\ell = \alpha_\ell/\beta_\ell = k_{s\ell}/k_{n\ell}$, $g_a = w_a/m_a = k_{na}N_f/k_{HDNa}$, and $g_\ell = w_\ell/m_\ell = k_{n\ell}N_f/k_{HDN\ell}$. Here the space time and residence time are both relevant to the analysis of the problem at hand.

References

[1] H. Topsøe, B.S. Clausen, F.E. Massoth, Hydrotreating Catalysis, Springer-Verlag, 1996.
[2] T. Kabe, A. Ishihara, W. Qian, Hydrodesulfurization and Hydrodenitrogenation, Wiley-VCH, New York, 1999.
[3] S. Eijsbouts, L.C.A. van den Oetelaar, R.R. van Puijenbroek, J. Catal. 229 (2005) 352.
[4] M.J. Girgis, B.C. Gates, Ind. Eng. Chem. Res. 30 (1991) 2021.
[5] M. Egorova, R. Prins, J. Catal. 225 (2004) 417.
[6] J.V. Lauritsen, S. Helveg, E. Lægsgaard, I. Stensgaard, B.S. Clausen, H. Topsøe, F. Besenbacher, J. Catal. 197 (2001) 1.
[7] J.V. Lauritsen, M. Nyberg, J.K. Nørskov, B.S. Clausen, H. Topsøe, E. Lægsgaard, F. Besenbacher, J. Catal. 224 (2004) 94.
[8] T.C. Ho, G.E. Markley, Appl. Catal. A: Gen. 267/1–2 (2004) 245.
[9] T.C. Ho, Catal. Today 98 (2004) 3.
[10] T.C. Ho, Catal. Today 130 (2008) 206.
[11] M. Breysse, E. Furimsky, S. Kasztelan, M. Lacroix, G. Perot, Catal. Rev. 44 (2002) 651.
[12] E. Furimsky, F.E. Massoth, Catal. Rev. 47 (2005) 297.
[13] E. Furimsky, F.E. Massoth, Catal. Today 52 (1999) 381.
[14] W. Kanda, I. Siu, J. Adjaye, A.E. Nelson, M.R. Gray, Energy Fuels 18 (2004) 539.
[15] I.A. Van Parijs, G.F. Froment, IEC Prod. Res. Dev. 25 (1986) 431.
[16] I.A. Van Parijs, L.H. Hosten, G.F. Froment, IEC Prod. Res. Dev. 25 (1986) 437.
[17] D.H. Broderick, B.C. Gates, AIChEJ 27 (1981) 663.
[18] G.F. Froment, L.C. Castaneda-Lopez, C. Marin-Rosas, Catal. Today 130 (2008) 446.
[19] T.C. Ho, J. Catal. 219 (2003) 442.
[20] T.C. Ho, D. Nguyen, J. Catal. 222 (2004) 450.
[21] T.C. Ho, D. Nguyen, Chem. Eng. Commun. 193 (2006) 460.
[22] G.H. Singhai, R.L. Espino, J.E. Sobel, G.A. Huff, J. Catal. 67 (1981) 457.
[23] C. Aubert, R. Durand, P. Geneste, C. Moreau, J. Catal. 112 (1988) 12.
[24] C. Schmitz, L. Datsevitch, A. Jess, Chem. Eng. Sci. 59 (2004) 2821.
[25] H. Yang, J. Chen, C. Fairbridge, Y. Briker, Y.J. Zhu, Z. Ring, Fuel Process. Technol. 85 (2004) 1415.
[26] H. Yang, J. Chen, Y. Briker, R. Szynkarczuk, Z. Ring, Catal. Today 109 (2005) 16.
[27] T.C. Ho, Catal. Rev. 50 (2008) 287.
[28] M. Sau, K. Basak, U. Manna, M. Santra, R.P. Verma, Catal. Today 109 (2005) 112.
[29] D. Yitzhaki, C. Aharoni, J. Catal. 107 (1987) 255.
[30] M. Sun, A.E. Nelson, J. Adjaye, J. Catal. 109 (2005) 49.
[31] T.C. Ho, Catal. Rev. 30 (1988) 117.
[32] J. Mijoin, V. Thévenin, N.A. Garcia, H. Yuze, J. Wang, W. Li, G. Pérot, J.L. Lemberton, Appl. Catal. A 180 (1999) 95.
[33] R.R. Chianelli, Catal. Rev. 26 (1984) 361.
[34] H. TopsØe, B.S. Clausen, N.-Y. TopsØe, E. Pedersen, W. Niemann, A. Müller, H. Bögge, B. Lengeler, J. Chem. Soc., Faraday Trans. I 83 (1987) 2157.
[35] T.C. Ho, US Patent 4,902,404, 1990.
[36] T.C. Ho, US Patent 4,973,397, 1990.
[37] K.H. Choi, Y. Sano, Y. Korai, I. Mochida, Appl. Catal. B: Environ. 53 (2004) 275.
[38] T.C. Ho, J. Sobel, Catal. Lett. 99 (2005) 109.